Spatial inhomogeneity of superconducting gap in epitaxial monolayer $FeTe_{1-x}Se_x$ films

Yaowu Liu,[1] Luxin Li,[2,*] Zheng Xie,[1] Zichun Zhang,[1] Sidan Chen,[1] Lichen Ji,[1] Wei Chen,[1] Xinyu Zhou,[1] Xiaopeng Hu,[1] Xi Chen,[1,3] Qi-Kun Xue,[1,4,5,3,†] and Shuai-Hua Ji[1,3,‡]

[1]*State Key Laboratory of Low-Dimensional Quantum Physics, Department of Physics, Tsinghua University, Beijing 100084, China*

[2]*Quantum Science Center of Guangdong-Hong Kong-Macao Greater Bay Area, Shenzhen 518048, China*

[3]*Frontier Science Center for Quantum Information, Beijing 100084, China*

[4]*Beijing Academy of Quantum Information Sciences, Beijing 100193, China*

[5]*Department of Physics, Southern University of Science and Technology, Shenzhen 518055, China*

(Received 13 July 2023; accepted 16 November 2023; published 11 December 2023)

Monolayer $FeTe_{1-x}Se_x$ films grown on a $SrTiO_3(001)$ substrate is a promising platform to explore both high-temperature and topological superconductivity. Using molecular beam epitaxy, we successfully synthesized monolayer $FeTe_{1-x}Se_x$ films ($0 \leqslant x \leqslant 1$) on a Nb-doped $SrTiO_3(001)$ substrate. The as-grown films with $0.30 \leqslant x \leqslant 1$ show superconductivity. By spatially mapping the superconducting gap distribution, we found a large gap variation of ∼3–7 meV. Our analysis shows that impurities/defects and local chemical composition variation play a minor role in the superconducting gap inhomogeneity. The large gap variation is possibly attributed to the joint effects of the interface inhomogeneity and inhomogeneous superfluid. Our study sheds light on the fundamental properties of two-dimensional iron-based superconductors.

DOI: 10.1103/PhysRevB.108.214514

I. INTRODUCTION

Both high-temperature and topological superconductors are the frontier subjects of condensed matter physics. The mechanism of high-temperature superconductivity still remains unresolved after several decades since its discovery, and solving the problem would have significant impacts on both basic science and practical technology. Meanwhile, topological superconductors are predicted to host Majorana bound states at the cores of vortices [1], thus providing a promising platform for topological quantum computing.

One of the promising candidates for a topological superconductor is $FeTe_{1-x}Se_x$. By employing angle-resolved photoemission spectroscopy, previous studies provided direct evidence of spin helical Dirac surface states as well as a superconductivity gap below the critical temperature in this material [2,3]. Signatures of Majorana bound states at the vortex core in an $FeTe_{0.55}Se_{0.45}$ single crystal were observed [4,5], which provides further evidence for the existence of topological superconductivity in this material. Apart from topological superconductivity, $FeTe_{1-x}Se_x$ also provides a promising platform to explore other exotic ordered phases such as a nematic phase where the rotation symmetry is broken [6–8].

The high-temperature superconductivity of monolayer FeSe grown on $SrTiO_3$, where the superconductivity gap is enhanced from about 2 meV of the bulk material to about 20 meV [9], has attracted intensive studies recently. Spectroscopic investigations found a gap opening temperature up to 90 K [10–15]. In addition, signatures of incoherent Cooper pairs and pseudogap phenomena that resemble the situation of cuprates [15] have been reported in this system. This interface-enhanced superconductivity provides a model system to explore the underlying mechanism of Cooper pairing in high-temperature superconductors.

Interface-enhanced superconductivity of monolayer $FeTe_{1-x}Se_x$ on $SrTiO_3$ has been reported by Li and co-workers [16]. In addition, a monolayer $FeTe_{1-x}Se_x$ thin film grown on a $SrTiO_3$ substrate is also predicted to be topological. Comparing with monolayer FeSe on a $SrTiO_3$ substrate, Te substitution in FeSe can increase the anion height and hence induce a band inversion at the Γ point, making the system topologically nontrivial [2,17]. A topological transition at an Se content of 33% was reported by Shi *et al.* [18]. So far the studies on monolayer $FeTe_{1-x}Se_x$ films are still scarce.

Here, we report the epitaxial growth of monolayer $FeTe_{1-x}Se_x$ ($0 \leqslant x \leqslant 1$) grown on Nb-doped $SrTiO_3$. By fine tuning the flux ratio between Se and Te, superconductivity in as-grown monolayer $FeTe_{1-x}Se_x$ ($0.30 \leqslant x \leqslant 1$) films has been achieved. We observe a large spatial variation of the superconducting order parameter (∼3–7 meV) in the whole superconducting regime and such a large variation persists even in the areas without impurities. Our analysis shows that impurities or defects introduced during growth, local chemical composition variation, and low dimensionality cannot fully account for this large variation of the superconducting gap. This large variation of the gap is possibly attributed to the joint effects of the inhomogeneity of the interface and the inhomogeneous superfluid. Our results indicate a strong inhomogeneity of superconductivity in iron-based superconductor thin films and shed light on the basic properties of an $FeTe_{1-x}Se_x$ monolayer on a $SrTiO_3$ substrate.

*liluxin@quantumsc.cn
†qkxue@mail.tsinghua.edu.cn
‡shji@mail.tsinghua.edu.cn

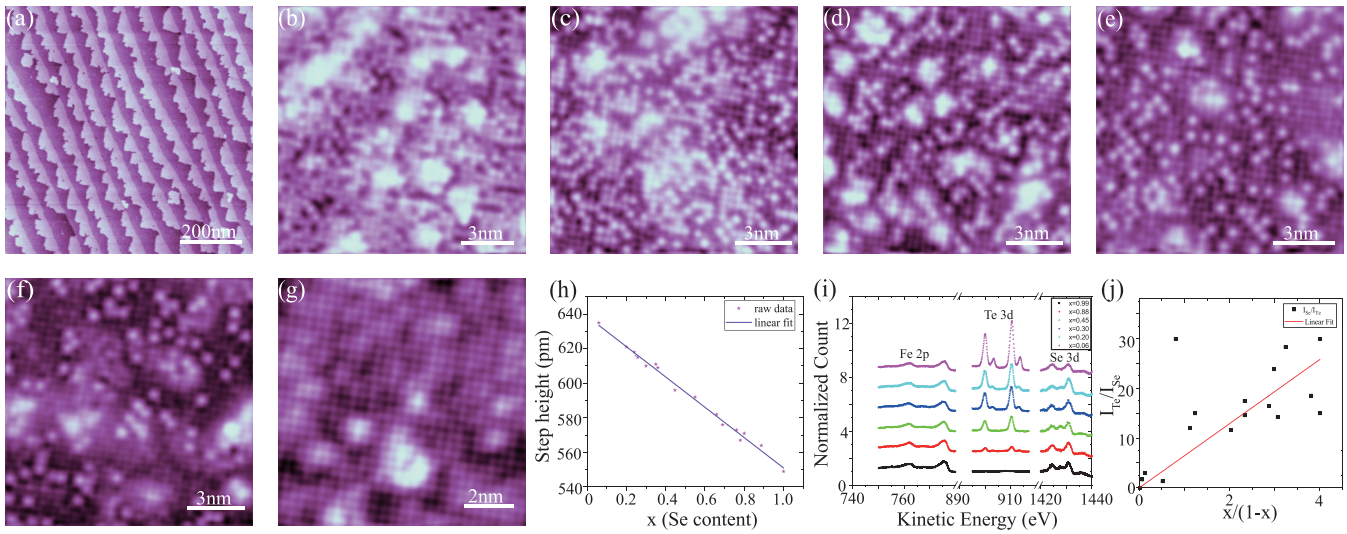

FIG. 1. (a) STM topography (500×500 nm, $I_t = 10$ pA, $V_b = 1$ V) of a typical as-grown $FeTe_{1-x}Se_x$ film. (b)–(g) Atomically resolved STM image for (b) $FeTe_{0.7}Se_{0.3}$ ($I_t = 500$ pA, $V_b = 30$ mV), (c) $FeTe_{0.47}Se_{0.53}$ ($I_t = 500$ pA, $V_b = 50$ mV), (d) $FeTe_{0.34}Se_{0.66}$ ($I_t = 500$ pA, $V_b = 50$ mV), (e) $FeTe_{0.2}Se_{0.8}$ ($I_t = 500$ pA, $V_b = 50$ mV), (f) $FeTe_{0.14}Se_{0.86}$ ($I_t = 300$ pA, $V_b = 30$ mV), and (g) FeSe ($I_t = 500$ pA, $V_b = 30$ mV). (h) Step heights as a function of Se content. (i) Normalized XPS data with the Shirley background deducted. (j) $\frac{I_{Te}}{I_{Se}}$ as a function of $\frac{1-x}{x}$.

II. EXPERIMENTAL DETAILS

The experiments were performed on a homemade low-temperature ultrahigh vacuum (UHV, 1×10^{-10} Torr) multiprobe scanning tunneling microscope (STM) equipped with molecular beam epitaxy [19]. The lowest temperature of the STM head could reach 4.7 K. Before epitaxial growth, the Nb-doped (0.05 wt.%) $SrTiO_3$(001) substrates were annealed at 1200 °C for 15 min, and the flux ratios of Fe, Se, and Te were checked by a quartz crystal microbalance (Inficon SQM-160). Then the $FeTe_{1-x}Se_x$ monolayer films were synthesized by codeposition of high-purity Fe (99.995%), Se (99.999%), and Te (99.999%) with the substrate held at 280 °C for 30 min and no postannealing was conducted (see Figs. S9 and S10 for the effect of postannealing [20]). High-quality monolayer $FeTe_{1-x}Se_x$ films without a phase separation, which usually occurs in a bulk single crystal [21,22], have been achieved by molecular beam epitaxial (MBE) growth on $SrTiO_3$ substrates. The minimized effect of phase separation is possibly due to the MBE growth process, which is far from a thermal equilibrium condition and dominated by the kinetic surface process, as well as the strain effect from the substrate [23,24]. A polycrystalline PtIr tip was used for the STM measurements, and the tunneling spectra were taken at 4.7 K using a standard lock-in technique with a bias modulation of 0.3 mV at 971 Hz. Then, the $FeTe_{1-x}Se_x$ monolayer films were transferred out for *ex situ* x-ray photoemission spectroscopy (XPS) measurements (Specs XPS system) with a photon energy of 1486.61 eV.

III. RESULTS AND DISCUSSION

In Fig. 1(a), we present a typical STM topography of $FeTe_{1-x}Se_x$ films, where we can observe fully covered monolayer films on the terrace and some additional second layer along the step edges of the substrate resulting from the step flow growth mode. It shows the high quality and flatness of the $FeTe_{1-x}Se_x$ films. The chemical composition of the films can be fine tuned by the flux ratio of Te and Se during the growth.

The exact x of $FeTe_{1-x}Se_x$ can be determined by atomically resolved images and *ex situ* XPS measurement. In the STM images of $FeTe_{1-x}Se_x$, because the apparent height of the Te atoms is larger than the Se atoms, x can be easily determined by counting the numbers of Te and Se atoms in the same images [25–27]. In order to precisely determine the Se content (x), we make an average of x of several areas from the same sample. In Figs. 1(b)–1(g), we present atomically resolved STM images of monolayer $FeTe_{1-x}Se_x$ films with x ranging from $x = 0.30$ to $x = 1$. As x increases, the concentration of Te atoms (brighter spots) in the images decreases. As shown in Fig. 1(h), the step heights extracted from films with different x show a negative linear relationship with x. This is consistent with the fact that the step heights should decrease from 0.64 nm of FeTe to 0.55 nm of FeSe with increasing x [28]. Core-level XPS can further prove the tuning of x in $FeTe_{1-x}Se_x$. Normalized XPS data of Fe 2p, Se 3d, and Te 3d orbitals are presented in Fig. 1(i). In order to compare the XPS data of different samples, we first extract the Shirley background and then we normalize each spectrum by dividing a constant fitted background. Then we use the ratio ($\frac{I_{Te}}{I_{Se}}$) between the integrated peak area of Te 3d and Se 3d peaks to determine how much Se content is in the sample [29]. By fitting $\frac{I_{Te}}{I_{Se}}$ with $\frac{1-x}{x}$, a linear relationship between them has been found. Both XPS and step height data suggest that the x determined by counting Te atoms is valid.

Next, we focus on the superconducting properties in the as-grown $FeTe_{1-x}Se_x$ films (see Fig. S8 for the averaged dI/dV of each monolayer $FeTe_{1-x}Se_x$ film [20]). In Figs. 2(a) and 2(b), we show the atomically resolved STM image of both $FeTe_{0.47}Se_{0.53}$ and FeSe, and we present the spatially resolved spectra in Figs. 2(c) and 2(d) along the dashed white

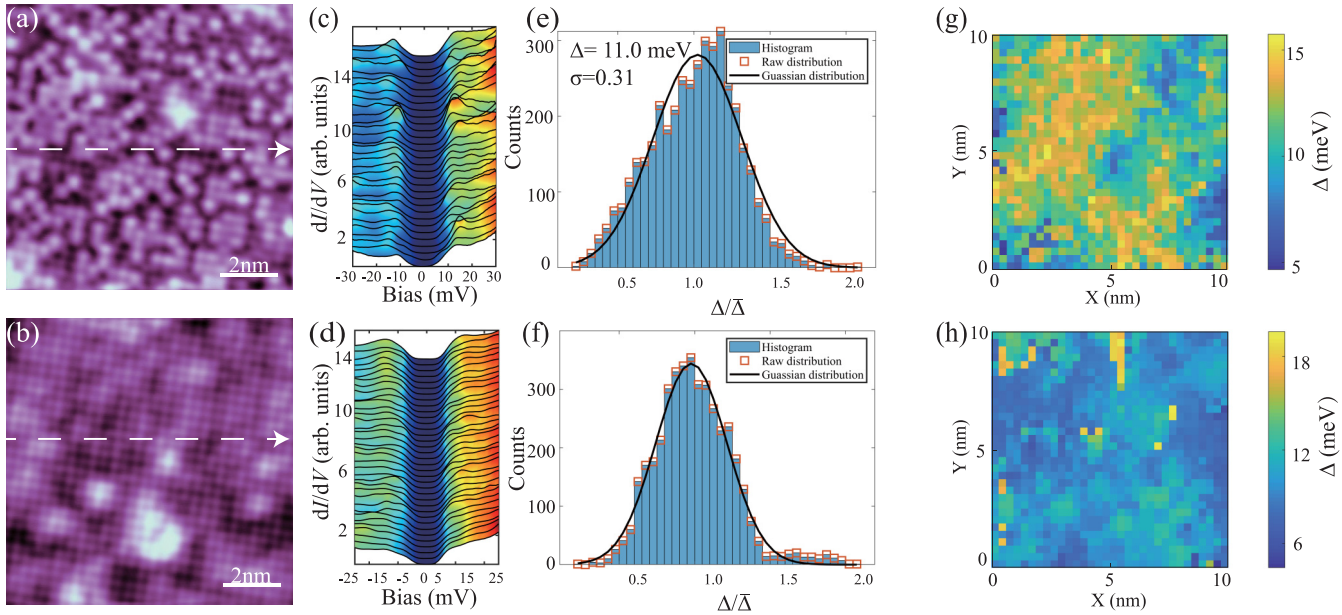

FIG. 2. (a), (b) Atomically resolved STM image ($I_t = 500$ pA, $V_b = 50$ mV) for $FeTe_{0.47}Se_{0.53}$ (10×10 nm) and FeSe (10×10 nm). (c), (d) Spatially resolved spectra along the white dashed arrow in (a) and (b), respectively. (c) $I_t = 200$ pA, $V_b = 30$ mV. (d) $I_t = 200$ pA, $V_b = 25$ mV. (e), (f) Statistics of gap distribution for $FeTe_{0.47}Se_{0.53}$ and FeSe. The black line is the Gaussian fit of the histogram. (g), (h) Superconducting gap map of (a) and (b), respectively.

arrow in Figs. 2(a) and 2(b). The spatially resolved spectra in $FeTe_{0.47}Se_{0.53}$ exhibit a large variation in the gap while that in FeSe is more uniform (see Fig. S7 for temperature-dependent dI/dV [20] and Ref. [30] therein). In order to statistically analyze such inhomogeneity, we measure the superconducting gap map at four to five different locations, which are randomly distributed. In pure FeSe samples, the superconducting gap map was collected on areas far away from the domain walls which would locally suppress the superconducting gap [31]. Using the BCS gap fit (see Fig. S1 for details [20] and Ref. [32] therein), the local superconducting gaps and the statistics are shown in Figs. 2(e) and 2(f). Both histograms of the gaps in the two samples are well fitted by a Gaussian distribution, yielding $\bar{\Delta} = 11.0$ meV, $\sigma = 0.31$ for $FeTe_{0.47}Se_{0.53}$ and $\bar{\Delta} = 9.5$ meV, $\sigma = 0.22$ for FeSe. Both samples exhibit a large variation in the superconducting gap. The gap maps for both samples are presented in Figs. 2(g) and 2(h), respectively, where the observation of the gap spatial inhomogeneity is more direct. In Fig. S2 of the Supplemental Material [20], we also present the map of zero-bias conductance (ZBC) where we can directly visualize impurity states. The azimuthally averaged autocorrelation between the map of ZBC and the gap shows a negative correlation (see Fig. S2 for detailed information [20]), which indicates impurity states tend to suppress the gap size.

To further investigate the inhomogeneity of the gap, we take the superconducting gap map at different areas and statistically analyze the gap distribution in $FeTe_{1-x}Se_x$ films with x ranging from $x = 0.30$ to $x = 1$. In order to exclude the influence of impurity states, we also statistically analyze the gap distribution in areas without impurity states. The detailed statistic results are presented in Fig. S3 [20] and are also summarized in Fig. 4(b). A large spatial variation of the superconducting gap exists in all samples with a magnitude from 3 to 7 meV [red square in Fig. 4(b)]. When we exclude the influence of impurities, such inhomogeneity is slightly suppressed, however, the variation is still very large (3–6 meV), as indicated by the blue pentagon in Fig. 4(b).

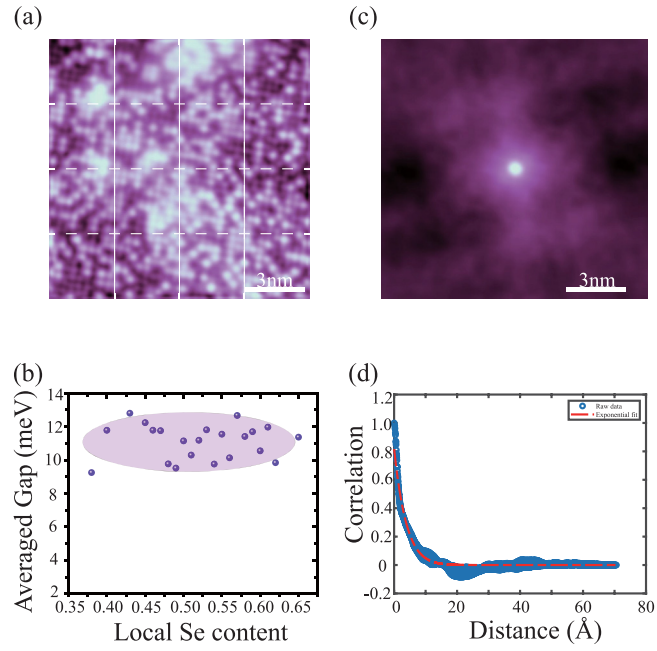

FIG. 3. (a) An example of a dissected atomically resolved STM image for $FeTe_{0.47}Se_{0.53}$ film (13×13 nm, $I_t = 500$ pA, $V_b = 50$ mV). We dissect the STM image along the dashed white lines and count the local Se content and the gap size inside each small box. (b) Averaged gap magnitude as a function of local Se content. (c) Autocorrelation of topography in (a). (d) Radial average of (c). The decay length is about 1.78 nm.

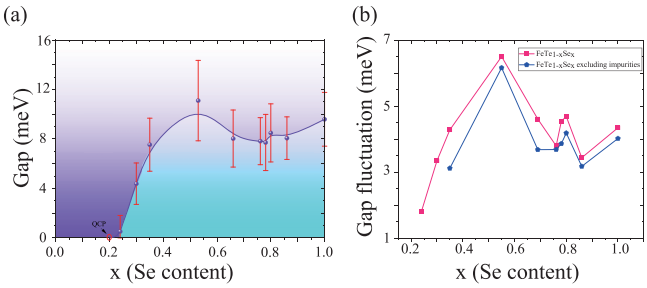

FIG. 4. (a) Phase diagram for monolayer $FeTe_{1-x}Se_x$. (b) Variation of the gap for as-grown films (red squares) and variation of the gap in areas without impurities (blue pentagons).

Next, we would like to discuss the origin of this large superconducting gap variation. The first reason coming to mind is the variation of local Se content due to the random distribution of Se and Te atoms, which locally distorts the anion height. So in order to investigate the influence of local Se content variation on superconductivity inhomogeneity, we take $FeTe_{0.47}Se_{0.53}$ as an example and dissect the atomically resolved STM image into small pieces containing areas of a length scale of 2–3 nm, as shown in Fig. 3(a). We carefully analyze the local content and the gap distribution of each area. The results are presented in Fig. 3(b) (see Fig. S4 for detailed information [20]) where we observe no obvious relation between the averaged gap value and the local Se content. This suggests that the local variation of Se content plays a minor role in the inhomogeneity of the superconducting gaps and is in agreement with previous work on single-crystal $FeTe_{0.4}Se_{0.6}$ [26]. To explain this, we first to investigate the length scale of inhomogeneity introduced by the chemical composition variation, which can be estimated using the autocorrelation of the atomically resolved topography. By radially averaging the autocorrelation map and then using an exponential fit, we can extract the length scale of the local chemical variation. The results for $FeTe_{0.47}Se_{0.53}$ film are shown in Figs. 3(c) and 3(d) and the length scale of inhomogeneity introduced by variation of the local chemical composition is about 1.78 nm, which is typical in all superconducting $FeTe_{1-x}Se_x$ films. The coherence length in this system is reasonably estimated using the coherence length of monolayer FeSe on a $SrTiO_3$ system which is about 2.5 nm [33] (this length can also be estimated by the correlation length of the autocorrelation of the superconducting gap—see Fig. S5 for details [20]). Since the length scale of inhomogeneity due to the variation of the local chemical composition is of the same order of coherence length of Cooper pairs, the local content variation should not exert a substantial influence on the inhomogeneity of the superconducting gap.

Another possibility is that there is inhomogeneity at the interface between the $FeTe_{1-x}Se_x$ film and the substrate. Homogeneity of the interface is essential to obtain homogeneous interface-enhanced superconductivity. Resembling the FeSe monolayer on $SrTiO_3$ [34–37], the interface also plays an important role in obtaining enhanced superconductivity in our $FeTe_{1-x}Se_x$ film. In light of that, any inhomogeneity present at the interface may introduce a spatial variation of superconductivity in epitaxial $FeTe_{1-x}Se_x$ films. On one hand, interface inhomogeneity may be caused by a disorder- or defect-induced inhomogeneous charge transfer between the interface and the monolayer films [10,13,38]. On the other hand, the inhomogeneity at the interface may arise from the inhomogeneous distribution of oxygen vacancies [39], which would influence the electron-phonon coupling effect [40–42] and in turn modulate the superconductivity locally.

Aside from the local variation of the chemical composition and inhomogeneous interface, a short coherence length may also play a role in the superconducting gap inhomogeneity. Superconductivity forms when phase coherent Cooper pairs condensate into a macroscopic quantum ground state. There are two energy scales in superconductivity: the single-particle gap Δ and the phase rigidity here denoted as $k_B T_\theta$. For conventional superconductors such as Pb, because the phase coherence length is usually very large (from hundreds of nanometers to micrometers), the phase rigidity is much larger than a single-particle gap [43]. However, for iron-based superconductors, the coherence length is much shorter (about several nanometers) [44–46], which puts the phase rigidity and pair breaking gap on the same energy scale. In single-crystal $FeTe_{0.55}Se_{0.45}$, Cho *et al.*, by taking advantage of scanning Josephson tunneling microscopy, found a strong inhomogeneity of the superfluid density [47]. They found such inhomogeneity is not caused by strong structural disorder nor inter-pocket scattering, and instead, they observe a correlation between the superfluid density and the local quasiparticle strength. In our case, the epitaxial monolayer $FeTe_{1-x}Se_x$ films also possess a short coherence length, so the short coherence length can also give rise to an inhomogeneous superfluid density. From our analysis, we find a weak negative correlation between the coherence peak height and superconducting gap (see Fig. S11 for more details [20]), which suggests that the inhomogeneous superfluid density possibly contributes to the spatial variation of the superconducting gap. However, we should point out that this correlation is almost absent in the bulk $FeTe_{0.55}Se_{0.45}$ [47] and the discrepancy between the bulk material and monolayer thin film is not clear currently.

Two dimensionality, on the other hand, might play a minor role in the spatial inhomogeneity of the superconducting gap in monolayer $FeTe_{1-x}Se_x$. For example, tetrabutyl ammonium (TBA^+) intercalated FeSe shows a sharp superconducting transition with T_{c0} up to about 40 K when its adjacent FeSe layer distance is enlarged from 5.5 Å in pristine FeSe to 15.5 Å by TBA^+ intercalation [48]. Although it is a highly two-dimensional system, its superconducting transition is even sharper than the monolayer FeSe/$SrTiO_3$ system. Moreover, a previous STM study on single atomic layer Pb and In on Si(111) also exhibits a uniform superconducting gap [49].

Figure 4(a) shows the superconducting phase diagram of monolayer $FeTe_{1-x}Se_x$, which shows a dome of an averaged superconducting gap as a function of x. Surprisingly, even in the sample of $FeTe_{0.76}Se_{0.24}$, there are scattered regions of the gap even reaching up to about 12 meV (see Fig. S6 for more details [20]). Also, the superconductivity emerges at $x \approx 0.20$ and the low Se content region, where patches of spectroscopic gap exist, could serve as a great platform to study the percolation of superconductivity. Meanwhile, $x \approx 0.2$ should be a quantum critical point where quantum fluctuations can lead to interesting physics. The averaged gap

reaches maximum at $x \approx 0.5$–0.6 and is slightly suppressed at $x \approx 0.8$ and then increases after this point. A dip of T_c was also observed in single-crystal $FeTe_{1-x}Se_x$ at $x \approx 0.81$ [50] which was ascribed to disorder in the samples. However, a decrease of T_c at $x \approx 0.7$ has also been reported and attributed to intrinsic nematic fluctuation [51].

IV. CONCLUSION

In summary, we have realized superconductivity in high-quality as-grown monolayer $FeTe_{1-x}Se_x$ films on $SrTiO_3$ without postannealing. Using a scanning tunneling microscope, we systematically measure and statistically analyze the distribution of the superconducting gap of monolayer $FeTe_{1-x}Se_x$ ($0.30 \leqslant x \leqslant 1$). We observe a large variation of the superconducting gap in all superconducting samples. Our analysis shows that impurities or defects introduced during growth and local chemical composition variation cannot fully account for this large variation in the superconducting gap. This spatial inhomogeneity of the superconducting gap is possibly attributed to the joint effects of the inhomogeneity of the interface and the inhomogeneous superfluid.

ACKNOWLEDGMENTS

We thank G.-M. Zhang for helpful discussions. This work is supported by the Ministry of Science and Technology of China (Grants No. 2021YFE0107900 and No. 2018YFA0305603) and the National Natural Science Foundation of China (Grants No. 12074211, No. 12141403, and No. 52388201).

[1] M. Sato and Y. Ando, Topological superconductors: a review, Rep. Prog. Phys. **80**, 076501 (2017).

[2] Z. Wang, P. Zhang, G. Xu, L. K. Zeng, H. Miao, X. Xu, T. Qian, H. Weng, P. Richard, A. V. Fedorov, H. Ding, X. Dai, and Z. Fang, Topological nature of the $FeSe_{0.5}Te_{0.5}$ superconductor, Phys. Rev. B **92**, 115119 (2015).

[3] P. Zhang, K. Yaji, T. Hashimoto, Y. Ota, T. Kondo, K. Okazaki, Z. Wang, J. Wen, G. D. Gu, H. Ding, and S. Shin, Observation of topological superconductivity on the surface of an iron-based superconductor, Science **360**, 182 (2018).

[4] D. Wang, L. Kong, P. Fan, H. Chen, S. Zhu, W. Liu, L. Cao, Y. Sun, S. Du, J. Schneeloch, R. Zhong, G. Gu, L. Fu, H. Ding, and H.-J. Gao, Evidence for Majorana bound states in an iron-based superconductor, Science **362**, 333 (2018).

[5] S. Zhu, L. Kong, L. Cao, H. Chen, M. Papaj, S. Du, Y. Xing, W. Liu, D. Wang, C. Shen, F. Yang, J. Schneeloch, R. Zhong, G. Gu, L. Fu, Y.-Y. Zhang, H. Ding, and H.-J. Gao, Nearly quantized conductance plateau of vortex zero mode in an iron-based superconductor, Science **367**, 189 (2020).

[6] T. Hanaguri, K. Iwaya, Y. Kohsaka, T. Machida, T. Watashige, S. Kasahara, T. Shibauchi, and Y. Matsuda, Two distinct superconducting pairing states divided by the nematic end point in $FeSe_{1-x}S_x$, Sci. Adv. **4**, eaar6419 (2018).

[7] R. Fernandes, A. Chubukov, and J. Schmalian, What drives nematic order in iron-based superconductors?, Nat. Phys. **10**, 97 (2014).

[8] H. Zhao, H. Li, L. Dong, B. Xu, J. Schneeloch, R. Zhong, M. Fang, G. Gu, J. Harter, S. D. Wilson *et al.*, Nematic transition and nanoscale suppression of superconductivity in Fe(Te,Se), Nat. Phys. **17**, 903 (2021).

[9] Q.-Y. Wang, Z. Li, W.-H. Zhang, Z.-C. Zhang, J.-S. Zhang, W. Li, H. Ding, Y.-B. Ou, P. Deng, K. Chang, J. Wen, C.-L. Song, K. He, J.-F. Jia, S.-H. Ji, Y.-Y. Wang, L.-L. Wang, X. Chen, X.-C. Ma, and Q.-K. Xue, Interface-induced high-temperature superconductivity in single unit-cell FeSe films on $SrTiO_3$, Chin. Phys. Lett. **29**, 037402 (2012).

[10] D. Liu, W. Zhang, D. Mou, J. He, Y.-B. Ou, Q.-Y. Wang, Z. Li, L. Wang, L. Zhao, S. He, Y. Peng, X. Liu, C. Chen, L. Yu, G. Liu, X. Dong, J. Zhang, C. Chen, Z. Xu, J. Hu *et al.*, Electronic origin of high-temperature superconductivity in single-layer FeSe superconductor, Nat. Commun. **3**, 931 (2012).

[11] J. J. Lee, F. T. Schmitt, R. G. Moore, S. Johnston, Y.-T. Cui, W. Li, M. Yi, Z. K. Liu, M. Hashimoto, Y. Zhang, D. H. Lu, T. P. Devereaux, D.-H. Lee, and Z.-X. Shen, Interfacial mode coupling as the origin of the enhancement of T_c in FeSe films on $SrTiO_3$, Nature (London) **515**, 245 (2014).

[12] Q. Song, T. L. Yu, X. Lou, B. P. Xie, H. C. Xu, C. H. P. Wen, Q. Yao, S. Y. Zhang, X. T. Zhu, J. D. Guo, R. Peng, and D. L. Feng, Evidence of cooperative effect on the enhanced superconducting transition temperature at the FeSe/$SrTiO_3$ interface, Nat. Commun. **10**, 758 (2019).

[13] S. He, J. He, W. Zhang, L. Zhao, D. Liu, X. Liu, D. Mou, Y.-B. Ou, Q.-Y. Wang, Z. Li, L. Wang, Y. Peng, Y. Liu, C. Chen, L. Yu, G. Liu, X. Dong, J. Zhang, C. Chen, Z. Xu *et al.*, Phase diagram and electronic indication of high-temperature superconductivity at 65 K in single-layer FeSe films, Nat. Mater. **12**, 605 (2013).

[14] Y. Xu, H. Rong, Q. Wang, D. Wu, Y. Hu, Y. Cai, Q. Gao, H. Yan, C. Li, C. Yin, H. Chen, J. Huang, Z. Zhu, Y. Huang, G. Liu, Z. Xu, L. Zhao, and X. J. Zhou, Spectroscopic evidence of superconductivity pairing at 83 K in single-layer FeSe/$SrTiO_3$ films, Nat. Commun. **12**, 2840 (2021).

[15] B. D. Faeth, S.-L. Yang, J. K. Kawasaki, J. N. Nelson, P. Mishra, C. T. Parzyck, C. Li, D. G. Schlom, and K. M. Shen, Incoherent cooper pairing and pseudogap behavior in single-layer FeSe/$SrTiO_3$, Phys. Rev. X **11**, 021054 (2021).

[16] F. Li, H. Ding, C. Tang, J. Peng, Q. Zhang, W. Zhang, G. Zhou, D. Zhang, C.-L. Song, K. He, S. Ji, X. Chen, L. Gu, L. Wang, X.-C. Ma, and Q.-K. Xue, Interface-enhanced high-temperature superconductivity in single-unit-cell $FeTe_{1-x}Se_x$ films on $SrTiO_3$, Phys. Rev. B **91**, 220503(R) (2015).

[17] X. Wu, S. Qin, Y. Liang, H. Fan, and J. Hu, Topological characters in $Fe(Te_{1-x}Se_x)$ thin films, Phys. Rev. B **93**, 115129 (2016).

[18] X. Shi, Z.-Q. Han, P. Richard, X.-X. Wu, X.-L. Peng, T. Qian, S.-C. Wang, J.-P. Hu, Y.-J. Sun, and H. Ding, $FeTe_{1-x}Se_x$ monolayer films: towards the realization of high-temperature connate topological superconductivity, Sci. Bull. **62**, 503 (2017).

[19] L. Li, C. Zheng, Y. Liu, X. Hu, S.-H. Ji, X. Chen, and Q.-K. Xue, Construction of molecular beam epitaxy and multi-probe scanning tunneling potentiometry combined system, Rev. Sci. Instrum. **90**, 093703 (2019).

[20] See Supplemental Material at http://link.aps.org/supplemental/10.1103/PhysRevB.108.214514 for detailed information of the BCS fit, zero-bias conductance map and their cross correlation with the gap, autocorrelation of the gap, the gap map of $FeTe_{0.76}Se_{0.24}$ film, temperature-dependent dI/dV of monolayer FeSe, average dI/dV of monolayer $FeTe_{1-x}Se_x$, and the postannealing effect.

[21] M. H. Fang, H. M. Pham, B. Qian, T. J. Liu, E. K. Vehstedt, Y. Liu, L. Spinu, and Z. Q. Mao, Superconductivity close to magnetic instability in $Fe(Se_{1-x}Te_x)_{0.82}$, Phys. Rev. B **78**, 224503 (2008).

[22] Y. Imai, Y. Sawada, F. Nabeshima, and A. Maeda, Suppression of phase separation and giant enhancement of superconducting transition temperature in $FeSe_{1-x}Te_x$ thin films, Proc. Natl. Acad. Sci. USA **112**, 1937 (2015).

[23] X. Niu, G. B. Stringfellow, and F. Liu, Phase separation in strained epitaxial InGaN islands, Appl. Phys. Lett. **99**, 213102 (2011).

[24] S. Y. Karpov, N. I. Podolskaya, I. A. Zhmakin, and A. I. Zhmakin, Statistical model of ternary group-III nitrides, Phys. Rev. B **70**, 235203 (2004).

[25] T. Hanaguri, S. Niitaka, K. Kuroki, and H. Takagi, Unconventional *s*-wave superconductivity in Fe(Se,Te), Science **328**, 474 (2010).

[26] U. R. Singh, S. C. White, S. Schmaus, V. Tsurkan, A. Loidl, J. Deisenhofer, and P. Wahl, Spatial inhomogeneity of the superconducting gap and order parameter in $FeSe_{0.4}Te_{0.6}$, Phys. Rev. B **88**, 155124 (2013).

[27] J.-X. Yin, Z. Wu, J.-H. Wang, Z.-Y. Ye, J. Gong, X.-Y. Hou, L. Shan, A. Li, X.-J. Liang, X.-X. Wu, J. Li, C.-S. Ting, Z.-Q. Wang, J.-P. Hu, P.-H. Hor, H. Ding, and S. H. Pan, Observation of a robust zero-energy bound state in iron-based superconductor Fe(Te,Se), Nat. Phys. **11**, 543 (2015).

[28] J. Zhuang, W. K. Yeoh, X. Cui, X. Xu, Y. Du, Z. Shi, S. P. Ringer, X. Wang, and S. X. Dou, Unabridged phase diagram for single-phased $FeSe_xTe_{1-x}$ thin films, Sci. Rep. **4**, 7273 (2014).

[29] X.-L. Peng, Y. Li, X.-X. Wu, H.-B. Deng, X. Shi, W.-H. Fan, M. Li, Y.-B. Huang, T. Qian, P. Richard, J.-P. Hu, S.-H. Pan, H.-Q. Mao, Y.-J. Sun, and H. Ding, Observation of topological transition in high-T_c superconducting monolayer $FeTe_{1-x}Se_x$ films on $SrTiO_3(001)$, Phys. Rev. B **100**, 155134 (2019).

[30] Y. Zhang, J. J. Lee, R. G. Moore, W. Li, M. Yi, M. Hashimoto, D. H. Lu, T. P. Devereaux, D.-H. Lee, and Z.-X. Shen, Superconducting gap anisotropy in monolayer FeSe thin film, Phys. Rev. Lett. **117**, 117001 (2016).

[31] W. Zhang, Z. Li, F. Li, H. Zhang, J. Peng, C. Tang, Q. Wang, K. He, X. Chen, L. Wang, X. Ma, and Q.-K. Xue, Interface charge doping effects on superconductivity of single-unit-cell FeSe films on $SrTiO_3$ substrates, Phys. Rev. B **89**, 060506(R) (2014).

[32] R. C. Dynes, V. Narayanamurti, and J. P. Garno, Direct measurement of quasiparticle-lifetime broadening in a strong-coupled superconductor, Phys. Rev. Lett. **41**, 1509 (1978).

[33] C. Chen, Q. Liu, W.-C. Bao, Y. Yan, Q.-H. Wang, T. Zhang, and D. Feng, Observation of discrete conventional Caroli–de Gennes–Matricon states in the vortex core of single-layer $FeSe/SrTiO_3$, Phys. Rev. Lett. **124**, 097001 (2020).

[34] H. Zhang, D. Zhang, X. Lu, C. Liu, G. Zhou, X. Ma, L. Wang, P. Jiang, Q.-K. Xue, and X. Bao, Origin of charge transfer and enhanced electron–phonon coupling in single unit-cell FeSe films on $SrTiO_3$, Nat. Commun. **8**, 214 (2017).

[35] Y. Zhou and A. J. Millis, Charge transfer and electron-phonon coupling in monolayer FeSe on Nb-doped $SrTiO_3$, Phys. Rev. B **93**, 224506 (2016).

[36] W. Zhao, M. Li, C.-Z. Chang, J. Jiang, L. Wu, C. Liu, J. S. Moodera, Y. Zhu, and M. H. Chan, Direct imaging of electron transfer and its influence on superconducting pairing at $FeSe/SrTiO_3$ interface, Sci. Adv. **4**, eaao2682 (2018).

[37] R. Peng, K. Zou, M. Han, S. D. Albright, H. Hong, C. Lau, H. Xu, Y. Zhu, F. Walker, and C. Ahn, Picoscale structural insight into superconductivity of monolayer $FeSe/SrTiO_3$, Sci. Adv. **6**, eaay4517 (2020).

[38] S. Tan, Y. Zhang, M. Xia, Z. Ye, F. Chen, X. Xie, R. Peng, D. Xu, Q. Fan, H. Xu, J. Jiang, T. Zhang, X. Lai, T. Xiang, J. Hu, B. Xie, and D. Feng, Interface-induced superconductivity and strain-dependent spin density waves in $FeSe/SrTiO_3$ thin films, Nat. Mater. **12**, 634 (2013).

[39] G. Gong, H. Yang, Q. Zhang, C. Ding, J. Zhou, Y. Chen, F. Meng, Z. Zhang, W. Dong, F. Zheng, P. Zhang, L. Yang, L. Gu, Q.-K. Xue, and L. Wang, Oxygen vacancy modulated superconductivity in monolayer FeSe on $SrTiO_{3-\delta}$, Phys. Rev. B **100**, 224504 (2019).

[40] Y. Xie, H.-Y. Cao, Y. Zhou, S. Chen, H. Xiang, and X.-G. Gong, Oxygen vacancy induced flat phonon mode at $FeSe/SrTiO_3$ interface, Sci. Rep. **5**, 10011 (2015).

[41] C. Chen, J. Avila, E. Frantzeskakis, A. Levy, and M. C. Asensio, Observation of a two-dimensional liquid of Fröhlich polarons at the bare $SrTiO_3$ surface, Nat. Commun. **6**, 8585 (2015).

[42] Z. Wang, S. McKeown Walker, A. Tamai, Y. Wang, Z. Ristic, F. Bruno, A. De La Torre, S. Riccò, N. Plumb, M. Shi, P. Hlawenka, J. Sanchez-Barriga, A. Varykhalov, T. K. Kim, M. Hoesch, P. D. King, W. Meevasana, U. Diebold, J. Mesot, B. Moritz *et al.*, Tailoring the nature and strength of electron-phonon interactions in the $SrTiO_3(001)$ 2D electron liquid, Nat. Mater. **15**, 835 (2016).

[43] V. Emery and S. Kivelson, Importance of phase fluctuations in superconductors with small superfluid density, Nature (London) **374**, 434 (1995).

[44] Y. Yin, M. Zech, T. L. Williams, X. F. Wang, G. Wu, X. H. Chen, and J. E. Hoffman, Scanning tunneling spectroscopy and vortex imaging in the iron pnictide superconductor $BaFe_{1.8}Co_{0.2}As_2$, Phys. Rev. Lett. **102**, 097002 (2009).

[45] L. Shan, Y.-L. Wang, B. Shen, B. Zeng, Y. Huang, A. Li, D. Wang, H. Yang, C. Ren, Q.-H. Wang, S. H. Pan, and H.-H. Wen, Observation of ordered vortices with Andreev bound states in $Ba_{0.6}K_{0.4}Fe_2As_2$, Nat. Phys. **7**, 325 (2011).

[46] G. Biswal and K. Mohanta, A recent review on iron-based superconductor, Mater. Today: Proc. **35**, 207 (2021).

[47] D. Cho, K. Bastiaans, D. Chatzopoulos, G. Gu, and M. Allan, A strongly inhomogeneous superfluid in an iron-based superconductor, Nature (London) **571**, 541 (2019).

[48] B. L. Kang, M. Z. Shi, S. J. Li, H. H. Wang, Q. Zhang, D. Zhao, J. Li, D. W. Song, L. X. Zheng, L. P. Nie, T. Wu, and X. H. Chen, Preformed Cooper pairs in layered FeSe-based superconductors, Phys. Rev. Lett. **125**, 097003 (2020).

[49] T. Zhang, P. Cheng, W.-J. Li, Y.-J. Sun, G. Wang, X.-G. Zhu, K. He, L. Wang, X. Ma, X. Chen, Y. Wang, Y. Liu, H.-Q. Lin,

J.-F. Jia, and Q.-K. Xue, Superconductivity in one-atomic-layer metal films grown on Si(111), Nat. Phys. **6**, 104 (2010).

[50] K. Terao, T. Kashiwagi, T. Shizu, R. A. Klemm, and K. Kadowaki, Superconducting and tetragonal-to-orthorhombic transitions in single crystals of $FeSe_{1-x}Te_x$ $(0 \leqslant x \leqslant 0.61)$, Phys. Rev. B **100**, 224516 (2019).

[51] K. Mukasa, K. Matsuura, M. Qiu, M. Saito, Y. Sugimura, K. Ishida, M. Otani, Y. Onishi, Y. Mizukami, K. Hashimoto, J. Gouchi, R. Kumai, Y. Uwatoko, and T. Shibauchi, High-pressure phase diagrams of $FeSe_{1-x}Te_x$: Correlation between suppressed nematicity and enhanced superconductivity, Nat. Commun. **12**, 381 (2021).